Phys Chem Minerals (2013) 40:29–40
DOI 10.1007/s00269-012-0543-7

ORIGINAL PAPER

Expansivity and compressibility of wadeite-type $K_2Si_4O_9$ determined by in situ high *T*/*P* experiments, and their implication

Linlin Chang · Zhiqiang Chen · Xi Liu · Hejing Wang

Received: 29 March 2012 / Accepted: 14 September 2012 / Published online: 26 September 2012

Abstract Wadeite-type $K_2Si_4O_9$ was synthesized with a cubic press at 5.4 GPa and 900 °C for 3 h. Its unit-cell parameters were measured by in situ high-*T* powder X-ray diffraction up to 600 °C at ambient *P*. The *T*–*V* data were fitted with a polynomial expression for the volumetric thermal expansion coefficient ($\alpha_T = a_0 + a_1T$), yielding $a_0 = 2.47(21) \times 10^{-5}$ K^{-1} and $a_1 = 1.45(36) \times 10^{-8}$ K^{-2}. Compression experiments at ambient *T* were conducted up to 10.40 GPa with a diamond-anvil cell combined with synchrotron X-ray radiation. A second-order Birch–Murnaghan equation of state was used to fit the *P*–*V* data, yielding $K_T = 97(3)$ GPa and $V_0 = 360.55(9)$ Å^3. These newly determined thermal expansion data and compression data were used to thermodynamically calculate the *P*–*T* curves of the following reactions: 2 sanidine ($KAlSi_3O_8$) = wadeite ($K_2Si_4O_9$) + kyanite (Al_2SiO_5) + coesite (SiO_2) and wadeite ($K_2Si_4O_9$) + kyanite (Al_2SiO_5) + coesite/stishovite (SiO_2) = 2 hollandite ($KAlSi_3O_8$). The calculated phase boundaries are generally consistent with previous experimental determinations.

L. Chang · X. Liu (✉) · H. Wang
Key Laboratory of Orogenic Belts and Crustal Evolution, Ministry of Education of China (MOE), Peking University, Beijing 100871, People's Republic of China
e-mail: xi.liu@pku.edu.cn

L. Chang · X. Liu · H. Wang
School of Earth and Space Sciences, Peking University, Beijing 100871, People's Republic of China

Z. Chen
National Synchrotron Light Source, Brookhaven National Laboratory, Upton, NY 11973, USA

Keywords Compressibility · Thermal expansivity · Thermodynamic calculation · Wadeite-type $K_2Si_4O_9$ · X-ray diffraction

Introduction

Potassium feldspar (orthoclase, abbreviated as Or hereafter; $KAlSi_3O_8$) is one of the most abundant minerals in the Earth's upper continental crust. Since it might be brought down to the Earth's interior via the subduction process (Armstrong and Harmon 1981; Dupre and Allegre 1983; Sobolev and Shatsky 1990; Hofmann 1997; Liu et al. 2010a), the physical and chemical behaviors of the composition $KAlSi_3O_8$ at high *P* have been extensively investigated by different methods. High-*P* experiments have been conducted to explore the subsolidus phase relations of this composition to about 130 GPa, the pressure along the core–mantle boundary of the Earth (Ringwood et al. 1967; Kinomura et al. 1975; Urakawa et al. 1994; Yagi et al. 1994; Tutti et al. 2001; Akaogi et al. 2004; Sueda et al. 2004; Nishiyama et al. 2005; Ferroir et al. 2006; Hirao et al. 2008), and reached good agreement, as suggested by the recent review of Liu et al. (2010a). On the other hand, thermodynamic calculations have been carried out to probe the high-*P* phase relations of this composition by using internally consistent thermodynamic datasets for the K_2O–Al_2O_3–SiO_2 ternary system, which have been long established and routinely updated (Geisinger et al. 1987; Fasshauer et al. 1998; Akaogi et al. 2004; Yong et al. 2006, 2008). Despite some small discrepancies such as the potential stability field of the phase assemblage coesite (Co)+ kalsilite (Fasshauer et al. 1998; Akaogi et al. 2004; Yong et al. 2006), the results from the thermodynamic calculations are consistent with the high-*P* experimental

discoveries. Additionally, theoretical simulations have also been attempted to constrain the physical properties of the high-*P* phases closely related to the Or composition, and valuable knowledge has been obtained (e.g. Mookherjee and Steinle-Neumann 2009; Boffa Ballaran et al. 2009; Caracas and Boffa Ballaran 2010; Deng et al. 2011).

However, a good agreement between the thermodynamic calculations and the direct experimental observations, at least theoretically, does not guarantee that the internally consistent thermodynamic dataset is problem-free. After Fasshauer et al. (1998) demonstrated the general agreement between the thermodynamic calculations and the high-*P* experimental results for the high-*P* phase relations of the Or composition, continuous effort has been made to revise the fundamental thermodynamic properties of the related phases, and important updates have been achieved (e.g. Zhang et al. 1993; Akaogi et al. 2004; Yong et al. 2006, 2008, 2012; Nishiyama et al. 2005; Ferroir et al. 2006; Liu et al. 2009, 2010b; Deng et al. 2011). The internal consistency of the thermodynamic database, the general agreement between the thermodynamic calculation and the experimental observation, and the updates of some important thermodynamic properties recently accomplished jointly indicate the inaccuracy, rather than accuracy, in some of the related thermodynamic data.

The role of a phase with the wadeite structure (space group $P6_3/m$) and the composition of $K_2Si_4O_9$ (the wadeite-type $K_2Si_4O_9$; Wd) in the high-*P* phase relations of the Or composition was first demonstrated by Kinomura et al. (1975). In the *P* range of about 5–10 GPa, it coexists with kyanite (Ky) and Co/stishovite (Sti), as revealed by later investigations (Urakawa et al. 1994; Yagi et al. 1994; Akaogi et al. 2004). Further, Swanson and Prewitt (1983) detailed its crystal structure (space group $P6_3/m$), Geisinger et al. (1987) conducted calorimetric measurements and vibrational calculations by using its infrared and Raman spectra, Fasshauer et al. (1998) measured its heat capacity in the *T* range of 195–598 K, Xu et al. (2005) calculated its enthalpy of formation from the drop solution enthalpy data of Akaogi et al. (2004), and Yong et al. (2008) obtained its low-*T* heat capacity data over the *T* range of 5–303 K. As pointed out by Akaogi et al. (2004), its thermal expansivity and compressibility (or bulk modulus), however, have not been very accurately determined. Indeed, the thermal expansivity was only tentatively constrained by experimental data at four temperatures (25, 200, 350 and 500 °C; Swanson 1986), while the bulk modulus was claimed to be about 90 GPa on the basis of some unpublished data of Ross, Swanson and Prewitt (Geisinger et al. 1987). It is obvious that more work on the thermal expansivity and compressibility of the Wd phase is required.

In this study, we synthesized the Wd phase, investigated its thermal expansivity by using in situ high-*T* powder X-ray diffraction (ambient *P*) and probed its compressibility by using powder synchrotron X-ray radiation (ambient *T*). With these new data, plus some recently updated thermodynamic data (e.g. Akaogi et al. 2011; Yong et al. 2012), we thermodynamically calculated some of the high-*P* phase relations related to the Or composition, which are independent to the corresponding phase relations directly constrained by early high-*P* experimental investigations.

Experimental

The Wd phase was synthesized by using a CS-IV 6 × 14 MN cubic press installed at the High-Pressure Laboratory of Peking University (Liu et al. 2012a). The experimental assembly BJC-1 was employed in the sample preparation, and its configuration details and *P* calibration were reported by Liu et al. (2012b). The experimental *T* was measured and controlled with a $Pt_{94}Rh_6$–$Pt_{70}Rh_{30}$ thermocouple (type B), with any potential *P* effect on its e.m.f. ignored. The starting material was prepared using reagent-grade chemicals (K_2CO_3 and SiO_2) with the following procedure. A mixture of K_2CO_3 and SiO_2 in a molar ratio of 1:4 was firstly homogenized under acetone in an agate mortar, secondly pressed into pellet with a stainless steel die, thirdly heated by using a conventional muffle furnace at 700 °C and 1 atm for about 72 h in order to remove CO_2, fourthly melted at 1,100 °C and 1 atm for 2 h in a Pt crucible hung with a Pt wire in a vertical furnace, and finally dropped into a bowl of water by cutting the Pt wire to quickly quench into a glass. The transparent product was examined with an optical microscopy, and no other phases were found. A few tiny pieces of the glass were mounted in epoxy, polished with a series of diamond pastes, washed with an ultrasonic washing machine, carbon-coated and examined with a JEOL JXA-8100 electron microprobe at the School of Earth and Space Sciences, Peking University. Although the glass was homogeneous, its composition is slightly short in K_2O, presumably due to the high-*T* volatilization of K_2O during the glass-making process (Table 1). The glass was finely crushed into a powder and stored in a drying oven at 110 °C for later high-*P* synthesizing experiments. The experimental conditions for synthesizing the Wd phase were arc-welded Pt capsule, and 5.4 GPa and 900 °C for 3 h. In total, three high-*P* synthesizing experiments were carried out at identical *P*–*T* conditions in order to generate enough material for subsequent power X-ray diffraction experiments.

Splits of the synthetic products from the high-*P* synthesizing experiments were processed and examined by a scanning electron microscope (SEM; Quanta 200 FEG), the JEOL JXA-8100 electron microprobe and a confocal

Table 1 Compositions of quenched glass, and wadeite-type $K_2Si_4O_9$ and coesite in high-*P* experimental products

Phase	SiO_2	Al_2O_3	Na_2O	K_2O
Glass(10)[a]	79.90(29)[b]	0.33(3)	0.01(1)	19.76(28)
Wd(27)	71.46(59)	0.09(6)	0.02(2)	28.43(62)
Co(14)	99.70(17)	0.07(6)	0.01(1)	0.23(12)

[a] The number in the parenthesis is the number of the electron microprobe analyses performed

[b] 79.90(29) should be read as 79.90 ± 0.29. All analyses from different splits of the glass or synthetic high-*P* products were put together and normalized to 100 wt% before average and standard deviation were calculated

micro-Raman system (Renishaw system RM-1000). In addition, the finely ground product was checked by a powder X-ray diffractometer hosted at the School of Earth and Space Sciences, Peking University (X'Pert Pro MPD system; Cu-$K\alpha$1 X-ray radiation).

In situ high-*T* powder X-ray diffraction experiments were conducted up to 750 °C at 1 atm. In these experiments, we used an X'Pert Pro MPD system with an attached Anton Paar HTK-1200 N oven, which ran with a Eurotherm temperature controller (Eurotherm 2604; type S thermocouple checked against the melting point of NaCl; Liu et al. 2010b). The accuracy in the *T* measurements with this heating system was previously evaluated up to 1,000 °C by using quartz as an internal standard (Hu et al. 2011); the variation patterns of the unit-cell parameters of quartz with *T* well reproduced the literature data (Carpenter et al. 1998), verifying the accuracy in the *T* measurements. Other details of the X'Pert Pro MPD diffractometer system included a Cu target, operation voltage of 40 kV and current of 40 mA. The heating and data collection procedures were as follows: after collecting the X-ray diffraction data at certain *T*, we raised the *T* to the next setpoint by 10 °C/min, and then kept it constant for 5 min to allow the material to relax before we started to collect the powder diffraction data at this new *T*. Since the Wd phase readily reverts to a glassy state, as experimentally demonstrated by Kinomura et al. (1975; ~700 °C in air for 6 h) and Swanson (1986; ~600 °C in air), long data collecting time at high *T* should be avoided. Consequently, our X-ray data were collected between 10 and 80°2θ only, with a scanning step width of 0.017°2θ and a counting time of 10 s for each scanning step. The alignment of the X-ray diffractometer system was done with a standard of silicon crystalline powder at ambient *T* only. Due to the thermal expansion of the furnace and sample holder components, the sample position was slightly changed at high *T*. Following the data processing procedure verified in He et al. (2011) and Wang et al. (2012), we used the MDI's program Jade 5.0 (Material Data, Inc.) to correct the influence of this small sample displacement by a full powder X-ray pattern refinement, which led to unit-cell parameters with high accuracy.

The high-*P* powder X-ray diffraction experiments at room *T* were carried out up to about 10 GPa with a symmetrical diamond-anvil cell (DAC) at the beamline X17C, National Synchrotron Light Source, Brookhaven National Laboratory. We used T301 stainless steel plates (initial thickness = 250 μm) as the gaskets. The central area of the plates was pre-indented (thickness = 40 μm), and a small hole (diameter = 160 μm) was electrically eroded. The experimental sample, plus a tiny ruby ball, was loaded into the hole in the gasket. The loaded *P* medium in our experiments was argon, which should solidify at ~1.2 GPa (Finger et al. 1981). Since solid argon is a very soft material with a bulk modulus less than 10 GPa (Finger et al. 1981; Ross et al. 1986), it should be able to provide a nearly hydrostatic pressure environment in our high-*P* experiments. Another advantage in using argon as the pressure medium is that it can be so readily detected by X-ray that its presence in the DAC experiments can be easily ascertained. Using the ruby fluorescence method (Mao et al. 1978), we measured the experimental *P* either before or after each X-ray analysis; the uncertainty in the *P* measurement was assumed as 0.1 GPa, considering the quasi-hydrostatic nature of the *P* state maintained by the pressure medium of argon. The incident synchrotron X-ray beam was monochromatized to a wavelength of 0.4066 Å, and its beam size was collimated to a size of about 25 × 20 μm^2. The X-ray diffraction pattern of the sample at certain *P* was collected with an exposure time of 20 min using an online CCD detector, and later integrated as a function of 2θ to give the conventional one-dimension X-ray profile using the Fit2D program. With a full profile refinement of the collected powder X-ray data, the positions of the diffraction peaks 100, 101, 102, 110, 111, 103, 201, 112, 113, 210, 121, 122, 300, 204, 123, 302, 220, 115, 124, 130, 006, 312, 125, 313, 224, 107, 117, 410, 135, 323 and 142 of the Wd phase were determined, and subsequently used to derive the unit-cell parameters at different pressures. These experimental and data processing techniques were well established and verified in our previous studies (Liu et al. 2008; Fleet et al. 2010).

Result and discussion

Stoichiometric Wd was successfully synthesized in spite of the shortage of K_2O in the starting material of the high-*P* synthesizing experiments, as revealed by our SEM data (Fig. 1), Raman data, powder X-ray diffraction data (Fig. 2) and electron microprobe analyses ($K_{2.02(5)}[Si_{3.99(1)}Al_{0.01(1)}]O_9$; Table 1). As expected, the excess of SiO_2 led to the formation

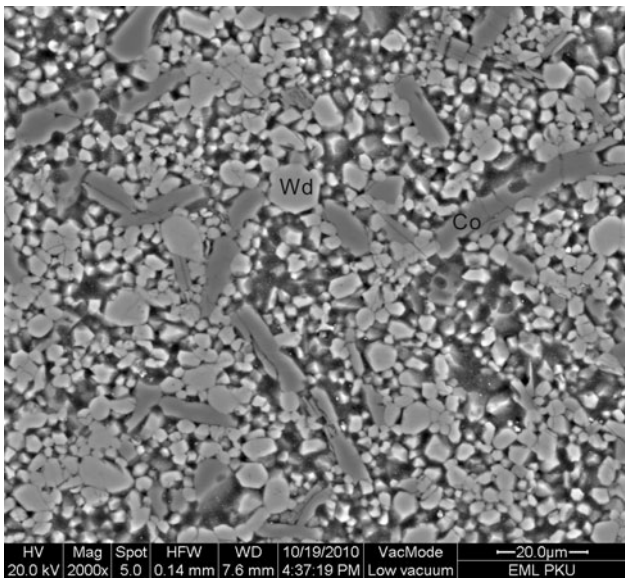

Fig. 1 Electron back-scatter image showing the texture of the experimental product synthesized at high-*P* and high-*T* conditions. Co, coesite; Wd, wadeite-type $K_2Si_4O_9$

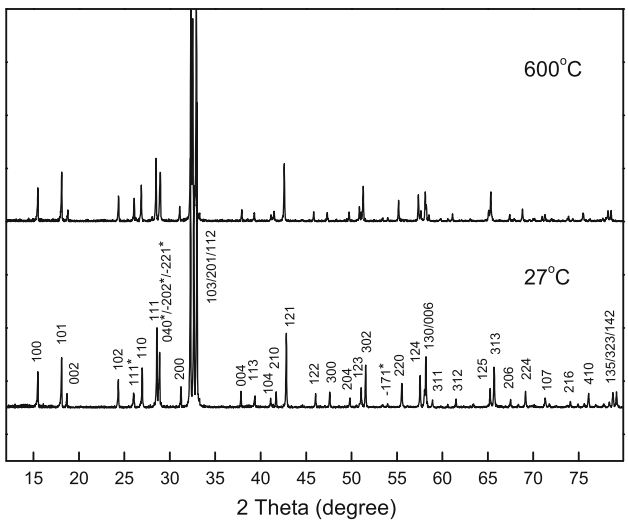

Fig. 2 Room-*P* XRD patterns of Wd at ambient *T* and 600 °C. The Bragg peaks of Co in the sample are denoted by *asterisks*

of Co. According to the compositions of the starting material, Wd and Co (Table 1), the phase proportion in the synthetic product should be approximately Wd/Co = 69.5:30.5 (by weight) or Wd/Co = 68.1:31.9 (by volume). The room-*T* and room-*P* unit-cell parameters of the Wd are $a = 6.6162(2)$ Å, $c = 9.5107(2)$ Å and $V = 360.55(2)$ Å^3, which are essentially identical to the values from the JCPDS reference pattern card 39-0212 (Swanson and Prewitt 1983) and other determinations in the literature (Kinomura et al. 1975; Fasshauer et al. 1998; Akaogi et al. 2004). In addition, the XRD pattern of Co was identical to that of the JCPDS reference pattern card 14-0654 (Zoltai and Buerger 1959).

Thermal expansivity of Wd at ambient *P*

High-*T* powder X-ray diffraction experiments were conducted up to 750 °C at ambient *P*. Since the diffraction peaks of the Wd phase began to disappear from 650 °C on, indicating the transformation from the crystalline form to the glassy form (Kinomura et al. 1975; Swanson 1986), we could obtain the unit-cell parameters with high accuracy up to 600 °C only (Table 2). In addition, some weak peaks from Co were also observed in the high-*T* X-ray data and used to extract the unit-cell parameters of Co at different *T*, which could be employed as an internal standard. Due to its very small thermal expansivity (Bourova et al. 2006), however, Co is a relatively poor internal standard. With the weak X-ray diffraction peaks from Co (Fig. 2), nevertheless, our observation made here is much comparable to the literature data (Fig. 3), confirming the accuracy of the *T* measurements in our experiments (Skinner 1966; Galkin et al. 1987; Bourova et al. 2006).

Figure 4 shows the variations of the unit-cell parameters *a*, *c*, *V* and *a/c* with *T*. In general, the dimension of the *c*-axis correlates almost linearly with *T*, but small deviation from a linear correlation might exist for the dimension of the *a*-axis and the volume. This observation is generally opposite to Swanson (1986). As *T* increases from 27 to 600 °C, the dimension of the *a*-axis increases by 0.85 %, that of the *c*-axis by 0.17 %, and the volume by 1.87 %. In addition, the *a/c* ratio increases from 0.6957 to 0.7004 for the same *T* range (about 0.7 %), indicating an anisotropic

Table 2 Unit-cell parameters of wadeite-type $K_2Si_4O_9$ at different temperatures and 1 atm

T (°C)	*a* (Å)	*c* (Å)	*V* (Å^3)	*a/c*
27	6.6162(2)[a]	9.5107(2)	360.55(2)	0.6957(1)
50	6.6184(1)	9.5110(2)	360.80(1)	0.6959(1)
100	6.6217(1)	9.5118(2)	361.19(1)	0.6962(1)
150	6.6266(1)	9.5135(1)	361.79(1)	0.6965(1)
200	6.6314(1)	9.5152(2)	362.38(1)	0.6969(1)
250	6.6359(2)	9.5172(3)	362.94(2)	0.6972(1)
300	6.6408(3)	9.5188(3)	363.55(3)	0.6977(1)
350	6.6462(3)	9.5202(4)	364.19(4)	0.6981(1)
400	6.6511(4)	9.5218(5)	364.79(5)	0.6985(1)
450	6.6567(4)	9.5229(5)	365.44(5)	0.6990(1)
500	6.6630(3)	9.5248(3)	366.21(3)	0.6995(1)
550	6.6678(3)	9.5257(5)	366.77(4)	0.7000(1)
600	6.6723(4)	9.5269(8)	367.31(5)	0.7004(1)

[a] The number in the parentheses represents one standard deviation in the rightmost digit

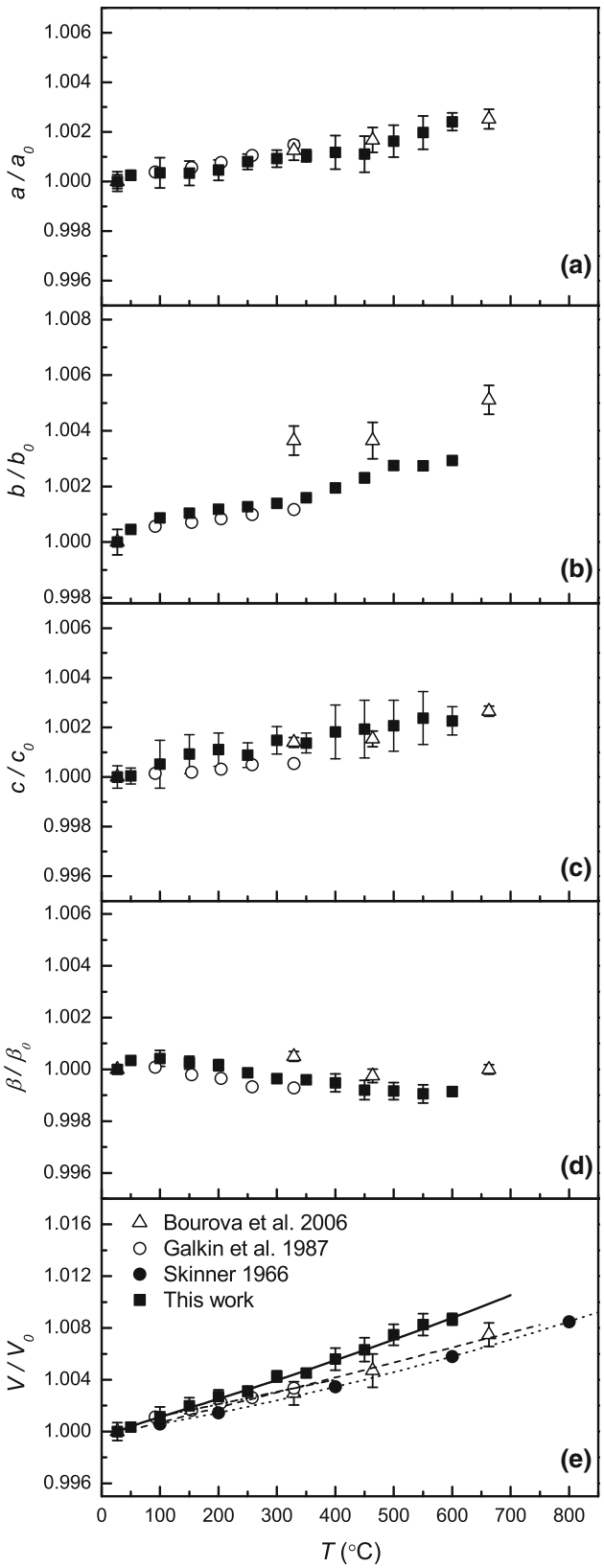

Fig. 3 Variation of the unit-cell parameters of Co with T: **a** the a-axis; **b** the b-axis; **c** the c-axis; **d** the β angle; **e** the volume

elasticity for the Wd phase. The T–V data have been fitted to the following equations:

$$V_T = V_0 \exp\left[\int_0^T \alpha_T dT\right] \quad (1)$$

and

$$\alpha_T = a_0 + a_1 T + a_2 T^{-2}, \quad (2)$$

where V_T, V_0 and α_T are the high-T volume, room-T volume and volumetric thermal expansion coefficient at temperature T, respectively. a_0, a_1 and a_2 are the constants obtained in fitting the experimental T–V data. Replacing the volume data in the equations above with the axial dimensions, the axial thermal expansion coefficients can be similarly obtained. In some cases, a_1 and a_2 could not be resolved due to the generally narrow T range in our experiments, and their values are therefore fixed as zero. The obtained parameters are the following: $a_0 = 2.47(21) \times 10^{-5}$ K^{-1} and $a_1 = 1.45(36) \times 10^{-8}$ K^{-2} for the volume; $a_0 = 1.50(2) \times 10^{-5}$ K^{-1} for the a-axis; $a_0 = 3.14(6) \times 10^{-6}$ K^{-1} for the c-axis. Apparently, the a-axis is much thermally expandable than the c-axis ($\alpha_{T\text{-}a}/\alpha_{T\text{-}c} = 4.8$ approximately). In comparison, the parameters determined by Swanson (1986) are the following: $a_0 = 2.94(5) \times 10^{-5}$ K^{-1} for the volume; $a_0 = 1.41(1) \times 10^{-5}$ K^{-1} for the a-axis; $a_0 = -2.4(5) \times 10^{-6}$ K^{-1}; and $a_1 = 6.6(9) \times 10^{-9}$ K^{-2} for the c-axis.

Compressibility of Wd at ambient T

The room-T compression experiments with the DAC did not suggest any phase transition (Fig. 5). The unit-cell parameters obtained from these experiments are summarized in Table 3. As P increases from 1 atm to 10.40 GPa, the a-axis decreases by 3.7 %, the c-axis by 2.1 % and the V by 9.1 %. Since the a-axis is more compressible than the c-axis, the a/c ratio decreases with P, by about 1.6 % for the experimentally covered P range. The relationship between the unit-cell parameters and P is detailed in Fig. 6; in all cases, an approximately linear correlation has been observed. In addition, Fig. 6 suggests that our P–V data are in good agreement with the equation of state of Wd claimed by Geisinger et al. (1987).

We fitted the P–V data to the second-order Birch–Murnaghan equation of state (EoS; Birch 1947) by a least-squares method:

$$P = 3K_T f_E (1 + 2f_E)^{\frac{5}{2}} \quad (3)$$

where P is the pressure, K_T the isothermal bulk modulus and f_E the Eulerian definition of finite strain. The Eulerian

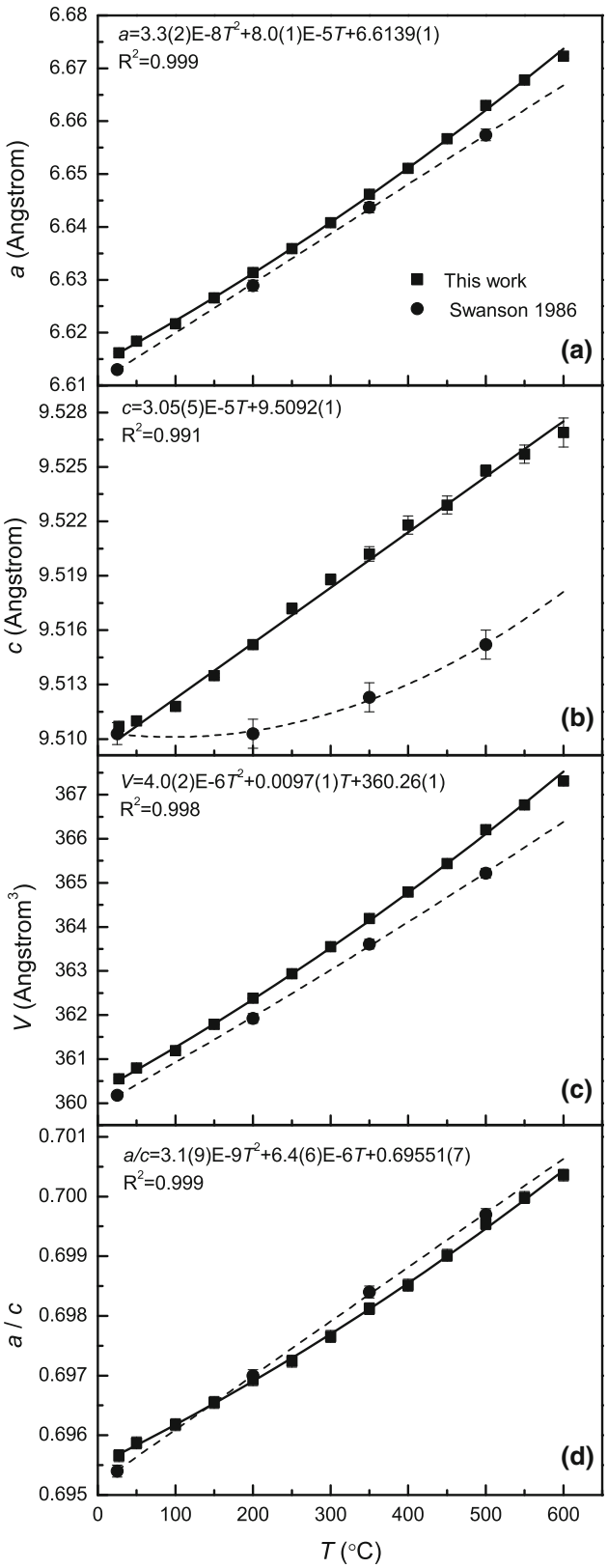

◀**Fig. 4** Variation of the unit-cell parameters of Wd with T at ambient P: **a** the a-axis; **b** the c-axis; **c** the volume; **d** the a/c ratio. The equations shown are empirically regressed from the data collected in this investigation. For comparison, the experimental data of Swanson (1986) were also plotted

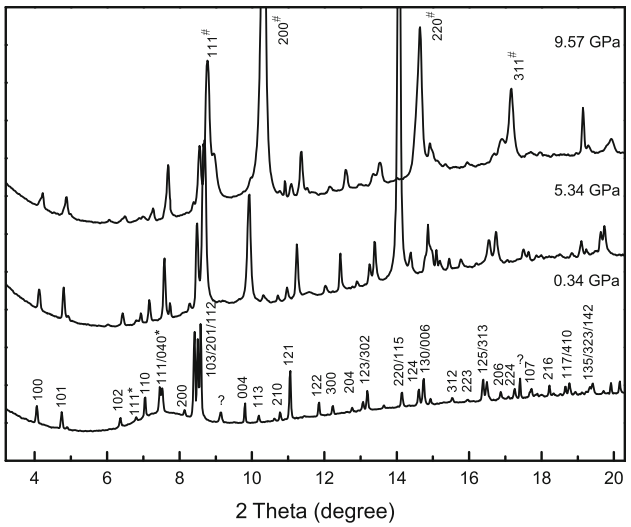

Fig. 5 Room-T XRD patterns of Wd at 0.34, 5.34 and 9.57 GPa. The Bragg peaks of Co in the sample are denoted by *asterisks*, and those of solid argon by *hashtags*. Two unknown peaks appearing in the XRD pattern at 0.34 GPa are denoted by *question* marks

Table 3 Unit-Cell parameters of wadeite-type $K_2Si_4O_9$ at different pressures and ambient temperature

P (GPa)	a (Å)	c (Å)	V (Å^3)	a/c
0.0001[a]	6.6162(2)[b]	9.5107(2)	360.55(2)	0.6957(1)
0.34(10)[c]	6.596(1)	9.497(2)	357.86(8)	0.6946(1)
0.75(10)	6.597(1)	9.495(2)	357.81(13)	0.6948(2)
1.51(10)	6.574(1)	9.482(3)	354.87(14)	0.6933(2)
3.89(10)	6.522(1)	9.449(3)	348.06(10)	0.6903(2)
5.34(10)	6.485(1)	9.430(1)	343.44(3)	0.6877(1)
7.54(10)	6.436(1)	9.387(1)	336.68(1)	0.6856(1)
9.57(10)	6.420(1)	9.357(2)	334.01(8)	0.6861(1)
10.40(10)	6.374(1)	9.312(2)	327.62(15)	0.6845(2)

[a] Data at room P were from conventional X-ray diffraction measurement, whereas those at high P were from DAC experiments

[b] The number in the parentheses represents one standard deviation in the rightmost digit

[c] Uncertainty in the P measurement at high P assumed to be 0.1 GPa, considering the quasi-hydrostatic nature of the P state maintained by the pressure medium of argon in the DAC experiments

definition of finite strain is $f_E = [(V_0/V)^{2/3} - 1]/2$, where V_0 is the volume at zero pressure and V the volume at high pressure. The fitting results are $K_T = 97(3)$ GPa and $V_0 = 360.55(9)$ Å^3, which broadly agree with the values claimed by Geisinger et al. (1987; $K_T = 90$ GPa and $V_0 = 360.11(7)$ Å^3).

In addition, a linearized second-order Birch–Murnaghan EoS (Angel 2000) was used to obtain the parameters of the

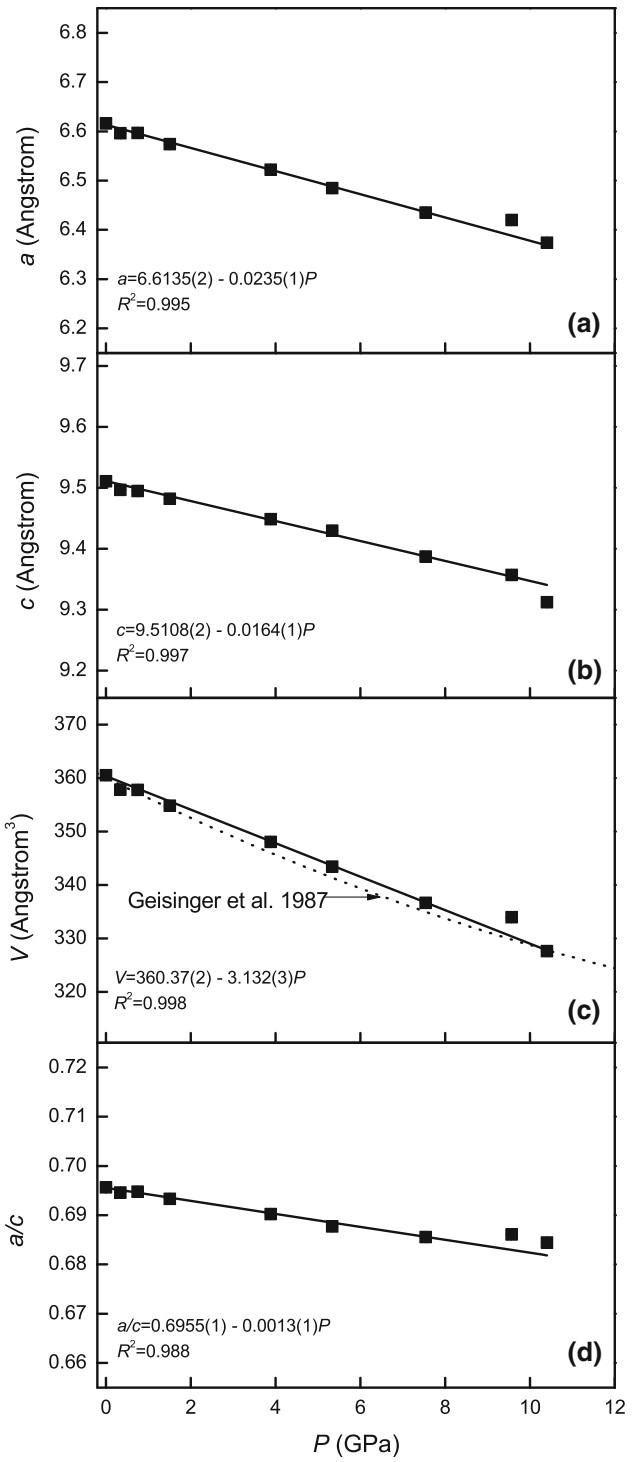

Fig. 6 Variation of the unit-cell parameters of Wd with P at ambient T: **a** the a-axis; **b** the c-axis; **c** the volume; **d** the a/c ratio. The equations shown are empirically regressed from the experimental data collected in this investigation. For comparison, the linear P–V correlation from Geisinger et al. (1987) is also plotted, with the zero-pressure volume from Swanson and Prewitt (1983). Note that the lengths of the error *bars* are generally equal to or smaller than the *symbols*

equations of state for the crystallographic axes ($K_{T\text{-}a}$ and $K_{T\text{-}c}$). The resulted EoS parameters are as follows: $K_{T\text{-}a} = 80(2)$ GPa and $a_0 = 6.6162(9)$ Å for the a-axis, and $K_{T\text{-}c} = 171(7)$ GPa and $c_0 = 9.511(1)$ Å for the c-axis. It follows that $K_{T\text{-}a}/K_{T\text{-}c} = 0.47$, indicating that the Wd phase at high P has an anisotropic elasticity as well.

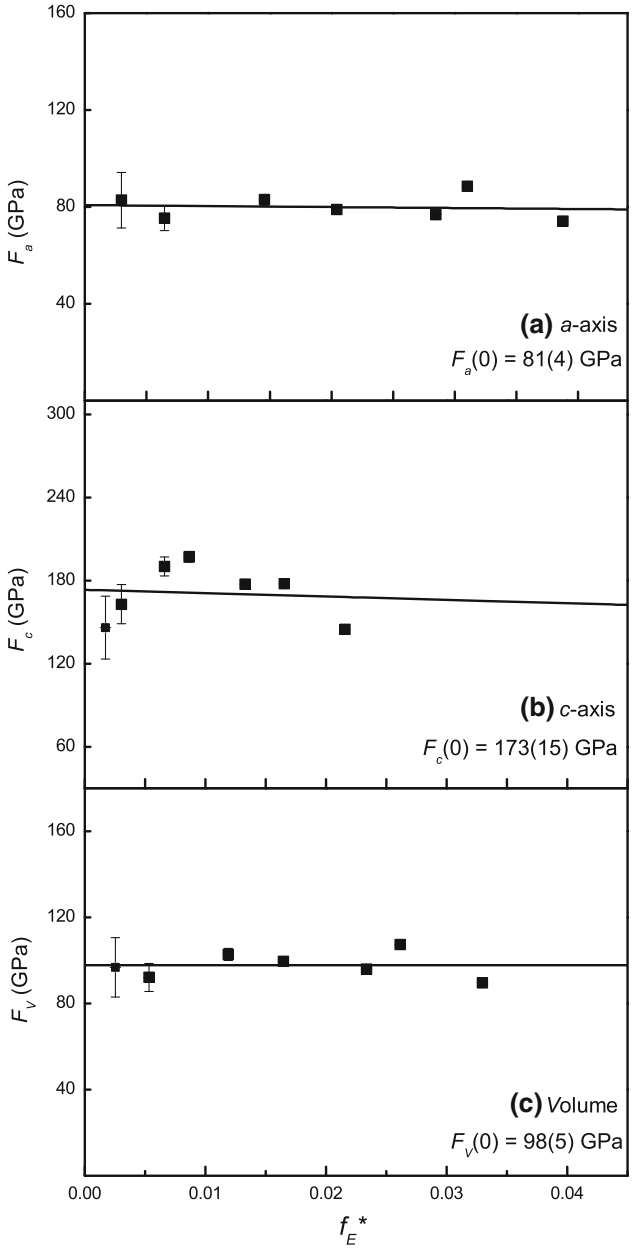

Fig. 7 Eulerian strain-normalized pressure (f_E^*-F) plot of Wd: **a** the a-axis; **b** the c-axis; **c** the volume. f_E^* stands for $f_{E,a}$ in (a), for $f_{E,c}$ in (b) and for $f_{E,V}$ in (c), which are the Eulerian definition of finite strain for the imaginary volume change along the a-axis, along the c-axis and volume, respectively. Estimated standard deviations have been calculated according to Heinz and Jeanloz (1984). The *solid lines* are the weighted linear fit through the data at $P > 0.5$ GPa

Alternatively, the linear compressibility (β_a and β_c) can be directly calculated from the unit-cell parameters at high P (Table 3), and the results are $\beta_a = 4.2(1) \times 10^{-3}$ and $\beta_c = 1.9(2) \times 10^{-3}$ GPa^{-1}. The ratio of the linear compressibilities, $\beta_a/\beta_c = 2.21$, again indicates an anisotropic elasticity for the Wd phase.

Whether the second-order Birch–Murnaghan EoS adequately fits the experimental data or not can be visionally evaluated by using the f_E–F plot (Fig. 7); F is defined as $F \equiv P/[3f_E(1 + 2f_E)^{5/2}]$. Using F, the third-order Birch–Murnaghan EoS can be rewritten as:

$$F = K_T + 3/2K_T\left(K_T^{'} - 4\right)f_E \quad (4)$$

so that the slope of the line defined by the experimental data should be equal to $3/2K_T\left(K_T^{'} - 4\right)$, and the intercept value is the isothermal bulk modulus. Accordingly, a slope of zero means $K_T^{'} = 4$, a negative slope $K_T^{'} < 4$ and a positive slope $K_T^{'} > 4$. Figure 7 suggests that all the slopes are close to zero, so that the second-order Birch–Murnaghan EoS is good enough to describe the compressional behavior of Wd.

Elastic anisotropy of Wd and its potential origin

Figure 8 compares the elastic behavior of the Wd phase at high-P and ambient-T conditions to that at ambient-P and high-T conditions. Clearly, the axial compressibility and thermal expansibility of the a-axis are simultaneously larger than those of the c-axis. In addition, all data points for the a-axis fall on an almost straight line, suggesting the effects of P and T on the a-axis are generally opposite to each other. In contrast, the data points for the c-axis do not behave in the same manner.

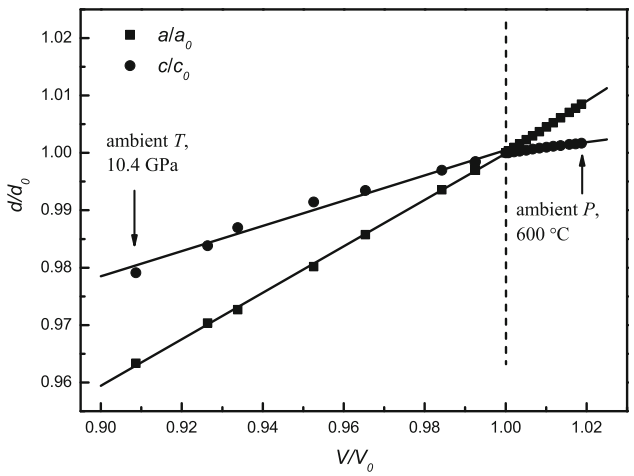

Fig. 8 Variation of the unit-cell dimensions (d/d_0) with V/V_0 of Wd. *Lines* are drawn to guide the eye

The elastic anisotropy of the Wd phase might be explained in terms of the framework topology of its structure (Fig. 9). The structure consists of layers of [Si_3O_9] rings parallel to the (001) plane, linked by isolated [SiO_6] octahedron via corner-sharing into a three-dimensional hexagonal framework (Swanson and Prewitt 1983; Xu et al. 2005). In general, the isolated [SiO_6] octahedron is very regular, indicating a potentially negligible role in the elastic behavior of the wadeite-type $K_2Si_4O_9$. On the other hand, the [SiO_4] tetrahedra, three of which form a [Si_3O_9] ring, are highly deformed, as manifested by the large difference in the bond lengths of O1–Si (1.64 Å) and O2–Si (1.61 Å), and in the bond angles of O1–Si–O1 (105.55°) and O2–Si–O2 (118.58°). The longer and weaker O1-Si bond in the (001) plane should lead to a larger thermal expansivity or compressibility in the a-axis

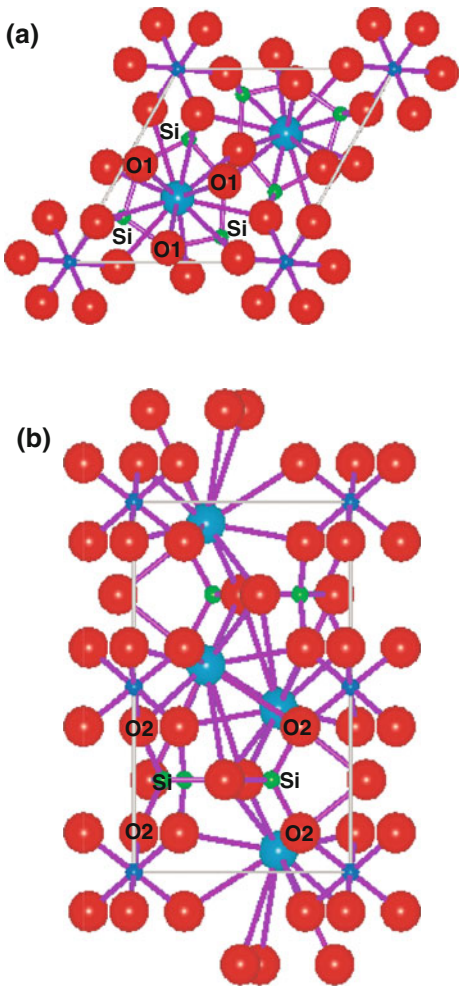

Fig. 9 Structure of Wd viewed down the [001] zone axis (**a**) and the [100] zone axis (**b**). small deep *green balls* represent the Si cations in the tetrahedra which form the [Si_3O_9] right in the plane (001), Small *blue balls* the Si cations in the octahedra, large light *blue balls* the K cations and large *red balls* the oxygens. Crystallographic data were from Swanson and Prewitt (1983)

direction. In addition, the larger O2–Si–O2 angle (generally normal to the plane (001)) between the [SiO_4] tetrahedron and [SiO_6] octahedron should be more reluctant to deform, compared to the O1–Si–O1 angle in the [Si_3O_9] ring which lies in the plane (001). Finally, the larger O2–Si–O2 angle might be much easier to be compressed than to be thermally expanded, which explains the apparent kink of the c/c_0–V/V_0 curve shown in Fig. 8. In contrast, the O1–Si–O1 angle in the plane (001) might freely increase or decrease, leading to the general linearity of the a/a_0–V/V_0 curve shown in Fig. 8.

Wd-related phase transitions at high *P*–*T* conditions

Previous high-*P* experimental work demonstrated that for the Or composition, the sequence of the stable phase assemblages from about 4–10 GPa is Sa, Co + Ky + Wd and $KAlSi_3O_8$-hollandite (Kinomura et al. 1975; Urakawa et al. 1994; Yagi et al. 1994); following Liu (2006), the $KAlSi_3O_8$-hollandite is termed as Holl-I in this study. The corresponding reactions are

$$2\ \mathrm{KAlSi_3O_8(Sa)} = \mathrm{K_2Si_4O_9(Wd)} + \mathrm{Al_2SiO_5(Ky)} + \mathrm{SiO_2(Co)}, \quad (5)$$

and

$$\mathrm{K_2Si_4O_9(Wd)} + \mathrm{Al_2SiO_5(Ky)} + \mathrm{SiO_2(Co/Sti)} = 2\ \mathrm{KAlSi_3O_8(Holl\text{-}I)}, \quad (6)$$

respectively. The potential stability field of the phase assemblage Co + kalsilite is not considered in this study since it might not exist at all (Fasshauer et al. 1998; Akaogi et al. 2004; Yong et al. 2006).

The newly determined volumetric thermal expansivity and compressibility of the Wd phase, along with other thermodynamic data directly measured by different types of experiments (Table 4), have been used to calculate the *P*–*T* curves of these reactions, according to Eq. 7:

$$\Delta G_r(P,T) = \Delta H^o_{r(T)} - T\Delta S^o_{r(T)} + \int_{1\mathrm{bar}}^{P} \Delta V_T(P)\mathrm{d}P + RT\ln K = 0 \quad (7)$$

where $\Delta G_r(P,T)$ is the Gibbs free energy change in the reaction at the interested P and T, $\Delta V_T(P)$ is the volume change in the reaction at interested P and T, $\Delta H^o_{r(T)}$ is the enthalpy of the reaction at 1 bar and the interested T, $\Delta S^o_{r(T)}$ is the entropy of the reaction at 1 bar and the interested T, R is the universal gas constant (8.3143 J K^{-1} mol^{-1}), P is the pressure, T is the temperature, and $K = 1$ for the present system with the Or composition since all the involved solid phases are essentially pure. The temperature dependencies of $\Delta H^o_{r(T)}$ and $\Delta S^o_{r(T)}$ are expressed by:

$$\Delta H^o_{r(T)} = \Delta H^o_{r(T_0)} + \int_{T_0}^{T} \Delta C_P(T)\mathrm{d}T, \quad (8)$$

and

$$\Delta S^o_{r(T)} = \Delta S^o_{r(T_0)} + \int_{T_0}^{T} [\Delta C_P(T)/T]\mathrm{d}T, \quad (9)$$

where $\Delta H^o_{r(T_0)}$ is the enthalpy of the reaction at 1 bar and the reference temperature, $\Delta S^o_{r(T_0)}$ is the entropy of the reaction at 1 bar and the reference temperature, $\Delta C_P(T)$ is the heat capacity, and T_0 is the reference temperature ($T_0 = 298$ K). In Eq. 7, the effect of T on the molar volume is calculated using the thermal expansion coefficients, and the effect of P is assumed to be T-independent and calculated using the second/third-order Birch–Murnaghan equation of state with corresponding bulk moduli (K_T) and pressure derivatives $\left(K'_T\right)$. The calculated *P*–*T* diagram is plotted in Fig. 10. For comparison, the phase boundaries determined by other researchers are also shown (Yagi et al. 1994; Urakawa et al. 1994; Akaogi et al. 2004; Yong et al. 2008, 2012). In general, the agreement among different investigations is good.

In the case of Eq. 5, all thermodynamic calculations suggest similar Clapeyron slopes (d*P*/d*T*) for the phase boundary between Sa and Wd + Ky + Co: 0.0025 GPa/ °C from this study and 0.0024(3) GPa/ °C from Akaogi et al. (2004) and Yong et al. (2008). The experimentally determined Clapeyron slopes (Yagi et al. 1994; Urakawa et al. 1994), however, are much smaller, which were apparently caused by the higher phase transition P at low T and lower phase transition P at high T, in comparison with the thermodynamic calculations (Fig. 10). Presumably, there were some small problems in the experimental studies such as the uncertainty in the P calibration as pointed out by Akaogi et al. (2004), ambiguity in identifying the equilibrium phases (Urakawa et al. 1994) and slow reaction rate at low T. In addition, careful and rigorous reversal high-P experiments were not conducted. On the other hand, our calculated phase-transition pressure is averagely lower by about 0.2 GPa than that determined by Akaogi et al. (2004), and by 0.3–0.4 GPa than that by Yong et al. (2008).

In the case of Eq. 6, the almost straight phase boundary between Wd + Ky + Co/Sti and Holl-I (Fig. 10) suggests that this phase transition is by no means significantly influenced by the phase transition between Co and Sti, in good agreement with Akaogi et al. (2004). Among the thermodynamics studies, the phase boundary calculated by Akaogi et al. (2004) locates at relatively low

Table 4 Physical properties of the phases used in the phase-boundary calculation

Phase	H^o_{298}	S^o_{298}	V^o_{298}	$\alpha = a_0 + a_1T + a_2T^{-2}$ (K^{-1})			K_T	K'_T	$C_P = c_1 + c_2T^{-0.5} + c_3T^{-2} + c_4T^{-3}$ (J mol^{-1} K^{-1})			
	(kJ mol^{-1})	(J mol^{-1} K^{-1})	(cm^3 mol^{-1})	$a_0 \times 10^5$	$a_1 \times 10^9$	a_2	(GPa)		$c_1 \times 10^{-2}$	$c_2 \times 10^{-3}$	$c_3 \times 10^{-6}$	$c_4 \times 10^{-8}$
Sa	−3,957.9(79)[a]	232.8(5)[b]	109.05[b]	1.297	8.683	0[c]	67[d]	4[e]	4.021	−2.629	−7.817	11.304[b]
Wd	−4,285.6(52)[a]	253.8(6)[f]	108.44[g]	2.47(21)	14.5(36)	0[h]	97(3)[h]	4[e]	4.991	−4.350	0	0[i]
Ky	−2,592.8(35)[a]	82.8(5)[b]	44.15[b]	1.76(25)	10.1(31)	0[j]	201(2)[k]	4[e]	2.450	−1.296	−7.080	8.322[b]
Co	−907.4(16)[a]	39.28(27)[l]	20.64[b]	0.543	8.32	−0.0061[c]	97.4[m]	4.3[m]	0.789	−0.164	−5.065	8.250[n]
Sti	−873.7(14)[a]	24.94[o]	14.02[p]	1.26(11)	12.9(17)	0[p]	296(5)[p]	4.2(4)[p]	0.873	−0.414	−2.735	2.207[q]
Holl-I	−3,793.7(60)[a]	166.2(2)[r]	71.28[s]	3.32	1.09	0[t]	183–0.033T[t]	4[e]	3.896	−1.823	−12.934	16.307[u]

Sa, sanidine; *Wd*, $K_2Si_4O_9$-type wadeite; *Ky*, kyanite; *Co*, coesite; *Sti*, stishovite; *Holl-I*, $KAlSi_3O_8$-hollandite

[a] Calculated from Akaogi et al. (1995, 2004)

[b] Robie and Hemingway (1995)

[c] Skinner (1966)

[d] Angel et al. (1988)

[e] Assumed

[f] Yong et al. (2008)

[g] Swanson and Prewitt (1983)

[h] This study

[i] Fasshauer et al. (1998)

[j] Liu et al. (2010b)

[k] Liu et al. (2009)

[l] Atake et al. (2000)

[m] Angel et al. (2001)

[n] Akaogi et al. (1995)

[o] Yong et al. (2012)

[p] Nishihara et al. (2005)

[q] Akaogi et al. (2011)

[r] Yong et al. (2006)

[s] Yamada et al. (1984)

[t] Nishiyama et al. (2005)

[u] Akaogi et al. (2004)

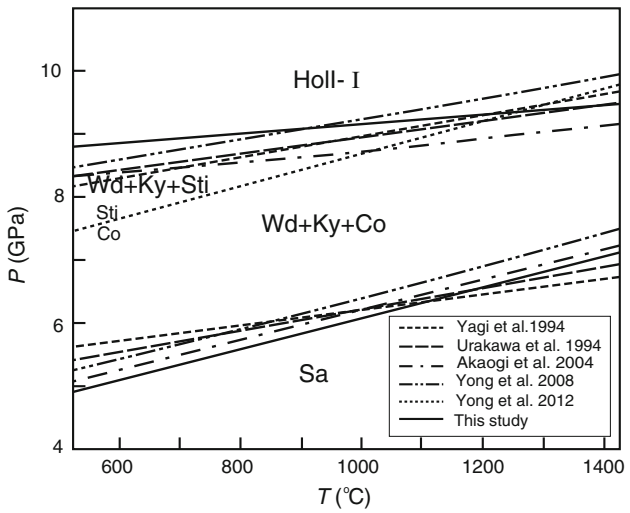

Fig. 10 Some phase relations in the composition of $KAlSi_3O_8$. Sa, Sanidine; Wd, wadeite-type $K_2Si_4O_9$; Co, coesite; Sti, stishovite; Holl-I, $KAlSi_3O_8$-hollandite. The phase boundary between Co and Sti was from Yong et al. (2012)

P (by ~0.5 GPa), and that obtained in this study has the smallest Clapeyron slope (0.0008 GPa/°C). In addition, the agreement between this study and Yong et al. (2008) is good, with the phase boundary from this study locating at slightly higher P at low T (by ~0.3 GPa at ~600 °C for example) but at slightly lower P at high T (by ~0.5 GPa at ~1,400 °C for example). On the other hand, our calculated phase boundary for the T interval of 1,000–1,400 °C agrees well with the experimental determination (Urakawa et al. 1994; Yagi et al. 1994), but locates at slightly higher P for the T interval of 600–1,000 °C.

It should be emphasized that our thermodynamic calculation has been carried out with the chemical and physical properties of the involving phases directly measured by different types of experiments only. Our results thus provide an independent evaluation to the high-P phase relations of the Or composition determined by the high-P experiments (Urakawa et al. 1994; Yagi et al. 1994). As shown in Fig. 10, the agreement between these two kinds of studies is good.

Acknowledgments We thank Professors Yingwei Fei and Youxue Zhang for their very constructive discussions. We are grateful to the useful comments on our manuscript from Dr Matteo Alvaro and an anonymous reviewer, and to the patience from Professor Masanori Matsui who editorially handled our paper. This investigation was financially supported by the National Natural Science Foundation of China (Grant #41090371) and the State Key Laboratory of Ore

Deposit Geochemistry, Institute of Geochemistry, Chinese Academy of Sciences (Grant #201114).

References

Akaogi M, Yusa H, Shiraishi K, Suzuki T (1995) Thermodynamic properties of α-quartz, coesite, and stishovite and equilibrium phase relations at high pressures and high temperatures. J Geophys Res 100:22337–22347

Akaogi M, Kamii N, Kishi A, Kojitani H (2004) Calorimetric study on high-pressure transitions in $KAlSi_3O_8$. Phys Chem Mineral 31:85–91

Akaogi M, Oohata M, Kojitani H, Kawaji H (2011) Thermodynamic properties of stishovite by low-temperature heat capacity measurements and the coesite-stishovite transition boundary. Am Mineral 96:1325–1330

Angel RJ (2000) Equation of state. In: Hazen RM, Downs RT (eds) High-Temperature and High-Pressure Crystal Chemistry. Reviews in Mineralogy and Geochemistry, vol 41. Mineralogical Society of America, Chantilly, pp 35–60

Angel RJ, Hazen RM, McCormick TC, Prewitt CT, Smyth JR (1988) Comparative compressibility of end-member feldspars. Phys Chem Mineral 15:313–318

Angel RJ, Mosenfelder JL, Shaw CSJ (2001) Anomalous compression and equation of state of coesite. Phys Earth Planet Inter 124: 71–79

Armstrong RL, Harmon RS (1981) Radiogenic isotopes: the case for crustal recycling on a near-steady-state no-continental-growth Earth [and discussion]. Philos Trans R Soc Lond A 301:443–472

Atake T, Inoue N, Kawaji H, Matsuzaka K, Akaogi M (2000) Low-temperature heat capacity of the high-pressure-phase of SiO_2, coesite, and calculation of the α-quartz-to-coesite equilibrium boundary. J Chem Thermodyn 32:217–227

Birch F (1947) Finite elastic strain of cubic crystals. Phys Rev 71:809–924

Boffa Ballaran T, Liu J, Dubrovinsky LS, Caracas R, Crichton W (2009) High-pressure ferroelastic phase transition in aluminosilicate hollandite. Phys Rev B 80:214104

Bourova E, Richet P, Petitet JP (2006) Coesite (SiO_2) as an extreme case of superheated crystal: an X-ray diffraction study up to 1776 K. Chem Geol 229:57–63

Caracas R, Boffa Ballaran T (2010) Elasticity of (K, Na)$AlSi_3O_8$ hollandite from lattice dynamics calculations. Phys Earth Planet Inter 181:21–26

Carpenter MA, Salje EKH, Graeme-Barber A, Wruck B, Dove MT, Knight KS (1998) Calibration of excess thermodynamic properties and elastic constant variations associated with the $\alpha \leftrightarrow \beta$ phase transition in quartz. Am Mineral 83:2–22

Deng L, Liu X, Liu H, Zhang Y (2011) A first-principles study of the phase transition from Holl-I to Holl-II in the composition $KAlSi_3O_8$. Am Mineral 96:974–982

Dupre B, Allegre CJ (1983) Pb-Sr isotope variation in Indian Ocean basalts and mixing phenomena. Nature 303:142–146

Fasshauer DW, Wunder B, Chatterjee ND, Höhne GWH (1998) Heat capacity of wadeite-type $K_2Si_4O_9$ and the pressure-induced stable decomposition of K-feldspar. Contrib Mineral Petrol 131:210–218

Ferroir T, Onozawa T, Yagi T, Merkel S, Miyajima N, Nishiyama N, Irifune T, Kikegawa T (2006) Equation of state and phase transition in $KAlSi_3O_8$ hollandite at high pressure. Am Mineral 91:327–332

Finger LW, Hazen RM, Zou G, Mao HK, Bell PM (1981) Structure and compression of crystalline argon and neon at high pressure and room temperature. Appl Phys Lett 39:892–894

Fleet ME, Liu X, Shieh SR (2010) Structural change in lead fluorapatite at high pressure. Phys Chem Mineral 37:1–9

Galkin VM, Dorochev AM, Babitch YuV (1987) Termitcheskoe raschirenie koesita. Izvestia A.N. SSSR. Geochimia 1645–1646

Geisinger KL, Ross NL, McMillan P, Navrotsky A (1987) $K_2Si_4O_9$: energetics and vibrational spectra of glass, sheet silicate, and wadeite-type phases. Am Mineral 72:984–994

He Q, Liu X, Hu X, Li S, Wang H (2011) Solid solution between lead fluorapatite and lead fluorvanadate apatite: mixing behavior, Raman feature and thermal expansivity. Phys Chem Mineral 38:741–752

Heinz DL, Jeanloz R (1984) The equation of state of the gold calibration standard. J Appl Phys 55:885–893

Hirao N, Ohtani E, Kondo T, Sakai T, Kikegawa T (2008) Hollandite II phase in $KAlSi_3O_8$ as a potential host mineral of potassium in the Earth's lower mantle. Phys Earth Planet Inter 166:97–104

Hofmann AW (1997) Mantle geochemistry: the message from oceanic volcanism. Nature 385:219–229

Hu X, Liu X, He Q, Wang H, Qin S, Ren L, Wu C, Chang L (2011) Thermal expansion of andalusite and sillimanite at ambient pressure: a powder X-ray diffraction study up to 1000 °C. Mineral Mag 75:363–374

Kinomura N, Kume S, Koizumi M (1975) Synthesis of $K_2SiSi_3O_9$ with silicon in 4- and 6-coordination. Mineral Mag 40:401–404

Liu X (2006) Phase relations in the system $KAlSi_3O_8$-$NaAlSi_3O_8$ at high pressure-high temperature conditions and their implication for the petrogenesis of lingunite. Earth Planet Sci Lett 246: 317–325

Liu X, Shieh SR, Fleet ME, Akhmetov A (2008) High-pressure study on lead fluorapatite. Am Mineral 93:1581–1584

Liu X, Shieh SR, Fleet ME, Zhang L (2009) Compressibility of a natural kyanite to 17.5 GPa. Prog Nat Sci 19:1281–1286

Liu X, Hu Z, Deng L (2010a) Feldspars under conditions of high temperature-high pressure. Acta Petrol Sin 26:3641–3650

Liu X, He Q, Wang H, Fleet ME, Hu X (2010b) Thermal expansion of kyanite at ambient pressure: an X-ray powder diffraction study up to 1000 °C. Geosci Front 1:91–97

Liu X, Chen J, Tang J, He Q, Li S, Peng F, He D, Zhang L, Fei Y (2012a) A large volume cubic press with a pressure-generating capability up to about 10 GPa. High Press Res 40:239–254

Liu X, Wang S, He Q, Chen J, Wang H, Li S, Peng F, Zhang L, Fei Y (2012b) Thermal elastic behavior of $CaSiO_3$-walstromite: a power X-ray diffraction study up to 900 °C. Am Mineral 97: 262–267

Mao HK, Bell PM, Shaner JW (1978) Specific volume measurements of Cu, Mo, Pt, and Au and calibration of ruby R1 fluorescence pressure gauge for 0.006 to 1 Mbar. J Appl Phys 49:3276–3283

Mookherjee M, Steinle-Neumann G (2009) Detecting deeply subducted crust from the elasticity of hollandite. Earth Planet Sci Lett 288:349–358

Nishihara Y, Nakayama K, Takahashi E, Iguchi T, Funakoshi K (2005) P-V-T equation of state of stishovite to the mantle transition zone conditions. Phys Chem Mineral 31:660–670

Nishiyama N, Rapp RP, Irifune T, Sanehira T, Yamazaki D, Funakoshi K (2005) Stability and P-V-T equation of state of $KAlSi_3O_8$-hollandite determined by in situ X-ray observations and implications for dynamics of subducted continental crust material. Phys Chem Mineral 32:627–637

Ringwood AE, Fredi AF, Wadsley AD (1967) High-pressure $KAlSi_3O_8$ and aluminosilicate with sixfold coordination. Acta Crystallogr 23:1093–1095

Robie RA, Hemingway BS (1995) Thermodynamic properties of minerals and related substances at 298.15 K and 1 bar (10^5 pascals) pressure and at higher temperatures. US Geol Survey Bull 2131:461

Ross M, Mao HK, Bell PM, Xu JA (1986) The equation of state of dense argon: a comparison of shock and static studies. J Chem Phys 85:1028–1033

Skinner BJ (1966) Thermal expansion. In: Clark SP (eds) Handbook of Physical Constants. Geol Soc Am Mem, pp 75–96

Sobolev NV, Shatsky VS (1990) Diamond inclusions in garnets from metamorphic rocks: a new environment from diamond formation. Nature 343:742–746

Sueda Y, Irifune T, Nishiyama N, Rapp RP, Ferroir T, Onozawa T, Yagi T, Merkel S, Miyajima N, Funakoshi KI (2004) A new high-pressure form of $KAlSi_3O_8$ under lower mantle conditions. Geophys Res Lett 31:L23612

Swanson DK (1986) High-temperature crystal chemical formalisms applied to $K_2Si^{VI}Si_3^{IV}O_9$ and $NaGaSi_3O_8$. PhD dissertation, State University of New York at Stony Brook

Swanson DK, Prewitt CT (1983) The crystal structure of $K_2Si^{VI}Si_3^{IV}O_9$. Am Mineral 68:581–585

Tutti F, Dubrovinsky LS, Saxena SK, Carlson S (2001) Stability of $KAlSi_3O_8$ hollandite-type structure in the Earth's lower mantle conditions. Geophys Res Lett 28:2735–2738

Urakawa S, Kondo T, Igawa N, Shimomura O, Ohno H (1994) Synchrotron radiation study on the high-pressure and high-temperature phase relations of $KAlSi_3O_8$. Phys Chem Mineral 21:387–391

Wang S, Liu X, Fei Y, He Q, Wang H (2012) In situ high-temperature powder X-ray diffraction study on the spinel solid solution $(Mg_{1-x}Mn_x)Cr_2O_4$. Phys Chem Mineral 39:189–198

Xu H, Navrotsky A, Lou Balmer M, Su Y (2005) Crystal-chemical and energetic systematics of wadeite-type phases $A_2BSi_3O_9$ (A=K, Cs; B=Si, Ti, Zr). Phys Chem Mineral 32:426–435

Yagi A, Suzuki T, Akaogi M (1994) High pressure transitions in the system $KAlSi_3O_8$-$NaAlSi_3O_8$. Phys Chem Mineral 21:12–17

Yamada H, Matsui Y, Ito E (1984) Crystal-chemical characterization of $KAlSi_3O_8$ with the hollandite structure. Mineral J 12:29–34

Yong W, Dachs E, Withers AC, Essene EJ (2006) Heat capacity and phase equilibria of hollandite polymorph of $KAlSi_3O_8$. Phys Chem Mineral 33:167–177

Yong W, Dachs E, Withers AC, Essene EJ (2008) Heat capacity and phase equilibria of wadeite-type $K_2Si_4O_9$. Contrib Mineral Petrol 155:137–146

Yong W, Dache E, Benisek A, Secco RA (2012) Heat capacity, entropy and phase equilibria of stishovite. Phys Chem Mineral 39:153–162

Zhang J, Ko J, Hazen RM, Prewitt CT (1993) High-pressure crystal chemistry of $KAlSi_3O_8$ hollandite. Am Mineral 78:493–499

Zoltai T, Buerger MJ (1959) The crystal structure of coesite, the dense, high-pressure form of silica. Z Kristallogr 111:129–141